Ionics (2019) 25:3623–3631
https://doi.org/10.1007/s11581-019-02960-3

ORIGINAL PAPER

Effects of $LiBF_4$ concentration in carbonate-based electrolyte on the stability of high-voltage $LiNi_{0.5}Mn_{1.5}O_4$ cathode

Yaohua Feng[1] · Hui Xu[1,2] · Yu Zhang[1] · Chunlei Li[1,2] · Dongni Zhao[1] · Qiuping Zhao[1,2] · Liping Mao[1,2] · Haiming Zhang[2] · Shiyou Li[1,2]

Received: 29 January 2019 / Revised: 27 February 2019 / Accepted: 5 March 2019 / Published online: 25 March 2019

Abstract

$LiBF_4$ has attracted much attention due to its better thermal stability, lower sensitivity to environmental humidity, and lower charge transfer resistance provided by its solution, especially at high voltage. Herein, the effects of the concentration of $LiBF_4$ salt on the stability and electrochemical properties of $LiNi_{0.5}Mn_{1.5}O_4$ (LNMO) cathode material have been investigated by using the mixed solvents of $LiBF_4$ salt, vinyl carbonate (EC), and diethyl carbonate (DEC) as electrolytes. The surface morphology and structure of cycled LNMO electrode are studied by scanning electron microscopy (SEM), Raman spectroscopy, and Fourier transform infrared spectroscopy (FTIR). The results show that the optimum concentration of $LiBF_4$ salt is 1.4 M $LiBF_4$-EC/DEC (1:5, by volume). Under optimum conditions, the LNMO cathode material has high electrochemical capacity and favorable rate performance. Meanwhile, the prepared electrolyte can easily form a thin and stable SEI film on the surface of LNMO electrode, which can effectively inhibit the continuous decomposition of the electrolyte.

Keywords Electrolyte · $LiBF_4$ · High voltage · $LiNi_{0.5}Mn_{1.5}O_4$ · Salt concentration

Introduction

With the increase of global energy demand, developing high energy storage devices has become an urgent problem to be solved. In energy storage devices, lithium-ion secondary batteries (LIBs) have been widely investigated and applied due to their relatively high specific energy density. Despite the energy density of LIBs being effectively improved, it still cannot meet the energy density requirements of energy storage devices, which hinders the large-scale application of LIBs [1]. Energy density is directly proportional to the working voltage of the battery, which is determined by the potential difference between cathode and anode [2]. The cut-off voltage of graphite [3] or silicon [4] is already near to 0 V vs. Li/Li^+, leaving no room for improvement of the anode potential; therefore, increasing the potential of the cathode is more promising. The materials such as $LiCoPO_4$ (4.8 V vs. Li/Li^+) [5, 6], $LiNiPO_4$ (5.1 V vs. Li/Li^+) [7], over-lithiated layered oxide (4.5 V vs. Li/Li^+) [8], $Li_3V_2(PO4)_3$ (4.8 V vs. Li/Li^+) [9], and $LiNi_{0.5}Mn_{1.5}O_4$ (4.7 V vs. Li/Li^+) [10, 11] have meet the demand of high voltage, but most of them have problems related to dislocation or dissolution of transition metal.

Among various high-voltage cathode materials, LNMO is one of the most promising candidates due to its high energy and power densities as well as being inexpensive and environmentally benign [12]. The high working potential (about 4 7 V vs. Li/Li^+) of Ni^{2+}/Ni^{3+} and Ni^{3+}/Ni^{4+} redox couples delivers an energy density equivalent to about 650 W h kg^{-1}, which is higher than that of the commercially available cathode materials such as $LiCoO_2$ (518 Wh kg^{-1}), $LiMn_2O_4$ (400 Wh kg^{-1}), $LiNi_{1/3}$ $Co_{1/3}Mn_{1/3}O_2$ (576 Wh kg^{-1}), and $LiFePO_4$ (495 Wh kg^{-1}) [13]. Furthermore, the three-dimensional channels in the spinel lattice enhance lithium diffusion rate during intercalation-deintercalation process. While the high operation voltage of LNMO increases power and energy density, it will also cause extensive oxidation of the conventional carbonate electrolytes, resulting in large

✉ Shiyou Li
sylilw@163.com

[1] College of Petrochemical Technology, Lanzhou University of Technology, 36 Pengjiaping Road, Lanzhou, Gansu Province, China

[2] Gansu Engineering Laboratory of Electrolyte for Lithium-ion Battery, Lanzhou 730050, China

irreversible capacity loss, low coulombic efficiency, and considerable thickening of the so-called solid-electrolyte interphase (SEI) layer [14].

The widespread use of $LiPF_6$ is attributed to its remarkable features including high solubility, good ionic conductivity, high dissociation constant, and satisfactory electrochemical stability. However, in the presence of trace water, the thermal stability and hydrolysis of $LiPF_6$ are poor, which seriously restricts the development of high-performance LIBs [15]. Compared with $LiPF_6$, $LiBF_4$ has the advantages of better thermal stability and lower sensitivity toward environmental moisture and its solution provides lower charge transfer resistance, especially at low temperatures [16]. Thus, in an effort to stabilize electrolyte solutions, $LiBF_4$ has often been studied as a candidate for $LiPF_6$ [17–19]. The BF_4^- anion has stronger inter- and intramolecular forces than its phosphorous-based analog. The B–F bond in $LiBF_4$ is less labile than the P–F bond in $LiPF_6$, resulting in improved hydrolytic and thermal stability of electrolyte solutions when $LiPF_6$ is replaced by $LiBF_4$ [18]. However, the ionic association between Li^+ and BF_4^- in electrolyte solutions is stronger than the ionic association between Li^+ and PF_6^-, resulting in lower conductivity, lower transport number, and poorer cation solvation [17]. Fortunately, the poor conductivity of $LiBF_4$ solutions does not impair the cycling performance even at sub-zero temperatures, as $LiBF_4$ apparently lowers charge transfer resistance (Rct) [19].

Recently, highly concentrated electrolyte solutions based on $LiBF_4$ have been reported to offer a wide potential window owing to the enhanced reductive and oxidative stability [20–22]. Takayuki Doi et al. [21] investigated that the 7.25 mol kg^{-1} $LiBF_4$/PC electrolyte can suppress the oxidative decomposition of electrolyte to reduce the irreversible capacity and improve rate capability due to a rapid interfacial Li^+ ion transfer rate at the $LiNi_{0.5}Mn_{1.5}O_4$/electrolyte interface. The 3.87 mol kg^{-1} $LiBF_4$/GBL electrolytes were used for charge/discharge reactions of graphite negative-electrodes and $LiNi_{0.5}Mn_{1.5}O_4$ positive-electrodes, which suppressed co-intercalation of solvent into graphite and reduced the polarization in charge/discharge reactions at $LiNi_{0.5}Mn_{1.5}O_4$ electrodes [20]. However, highly concentrated electrolyte solutions commonly have serious problems in high viscosities and high costs [22, 23]. Thus, it is necessary to optimize the concentration of lithium salt in solution.

Besides lithium salt, physicochemical properties of electrolyte, such as viscosity, liquid range, ionic conductivity, solubility, and electrochemical window, are greatly influenced by solvent system, including the solvent type and ratio [24].

In this study, an optimized electrolyte system was established by using the mixed solution of vinyl carbonate (EC) and diethyl carbonate (DEC) as solvents and $LiBF_4$ as solute to prevent electrolyte from decomposing at high voltage.

Experimental

Material preparation

$LiBF_4$ was purchased from Macklin Co., Ltd. EC, and DEC was bought from Chaoyang Yongheng Chemical Co., Ltd. The volume ratio of EC/DEC was selected as 5:1, 4:2, 3:3, 2:4, and 1:5, respectively. $LiBF_4$ salt concentrations were varied as 1.0, 1.2, 1.4, and 1.6 M in the electrolyte with optimum solvent ratio. All electrolytes were prepared in an argon atmosphere glove box (O_2, $H_2O < 1$ ppm).

The LNMO was purchased from Hunan Shanshan Advanced Material Co., Ltd. LNMO; acetylene black and poly (vinyl difluoride) (PVDF) were mixed at a weight ratio of 84:8:8 in N-methyl-pyrrolidone (NMP) solvent to prepare a slurry. The slurry was coated on Al foil and then heated in a vacuum oven at 120 °C for 12 h. The experimental coin cells (2032 type) were assembled in an argon atmosphere glove box using the abovementioned electrolytes as the electrolyte, lithium metal as the reference electrodes, and Celgard (2400) porous polypropylene as the separator.

Characterization

Electrochemical performance tests were carried out on a LAND CT2001A tester (Wuhan, China) in the voltage ranges of 3.5–5 V.

The electrochemical window was measured for the linear sweep voltammetry (LSV) in a three-electrode system with a stainless sheet as working electrode, lithium sheets respectively as counter electrode and reference electrode, at the scanning rate of 2 mV s^{-1} in the range of 3.0–7.0 V. All the measurements of each electrolyte formulation were repeated three times to ensure the validity of the obtained results.

Electrochemical impedance spectroscopy (EIS) spectra were measured in three-electrode cells through CHI660C electrochemical analyzer (Shanghai, China). The impedance measurements were respectively measured at the fully delithiated state of 5 V, with a sinusoidal AC perturbation of 5 mV in a frequency range from 100 kHz to 10 MHz.

The morphologies of SEI film were measured through a scanning electron microscope (SEM) (JSM5600). The structure of surface was analyzed with Raman spectra and Fourier transform infrared spectroscopy (FTIR). Prior to these surface analyses, the electrodes of the experimental cells were stripped off from electrodes in an Ar glove box, rinsed with DMC solvent five times to remove electrolyte from electrode, and dried in a vacuum drying for 12 h at 80 °C to remove the residual solvent of DMC.

Results and discussion

The optimization of solvent ratio

To optimize the appropriate solvent system, the electrochemical window of 1 M $LiBF_4$-EC/DEC electrolytes with solvent ratios of 5:1, 4:2, 3:3, 2:4, and 1:5 were investigated by LSV measurement, respectively (Fig. 1). The results show that the current density of all the electrolytes increases slowly below 5 V vs. Li/Li^+ indicating that these solvent systems would be alternative electrolytes for high-voltage LIBs. In addition, the decomposition voltage of electrolyte enhances gradually as the increase of DEC content. Paying special attention to the indispensable function of cyclic carbonate solvent of EC, 1:5 is selected as the optimized solvent ratio. This system has a high decomposition potential of ~ 5.9 V and would be regarded as an excellent candidate electrolyte for LIBs.

The electrochemical performance of $LiBF_4$ electrolyte with different lithium salt concentrations

The electrochemical stability

To evaluate the oxidation potential of $LiBF_4$ electrolyte at different concentrations, the electrochemical stabilities of the four electrolytes were investigated by LSV as shown in Fig. 2. Although electrolyte with 1.4 M $LiBF_4$ shows the best stability against oxidative decomposition, the active mechanism is unclear. The interaction between lithium salt and solvent is investigated and the mechanism is discussed in this study.

Self-discharge behaviors are highly associated with interfacial stability. At this stage, the loss of electrons in the electrolyte is encouraged and the overall electrode potential is reduced, making the electrodes more stable. The electrolyte

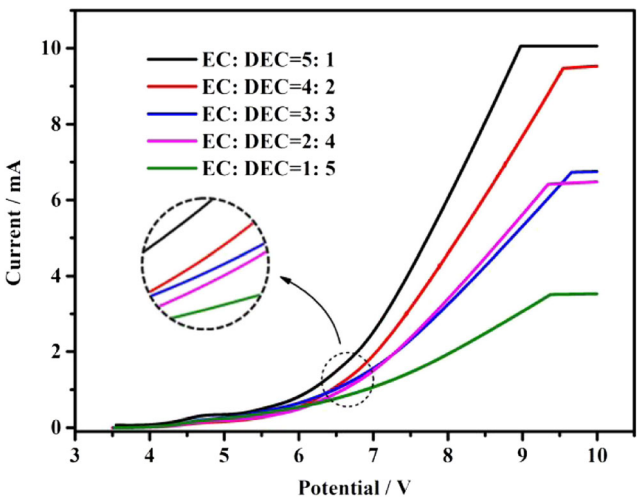

Fig. 1 The LSV curves of 1 M $LiBF_4$-EC/DEC electrolyte with different solvent ratios

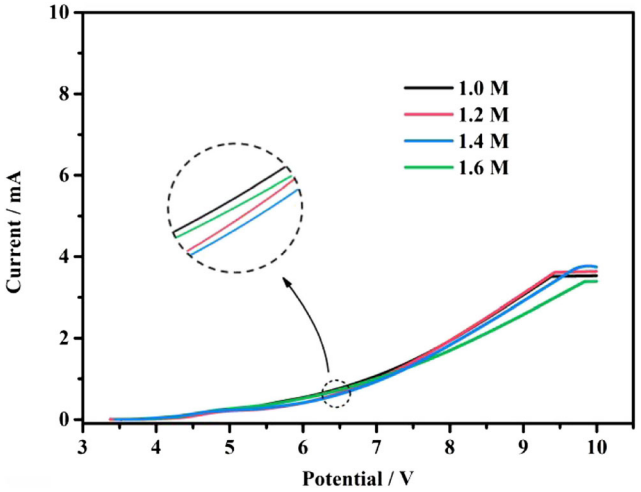

Fig. 2 The LSV of $LiBF_4$ electrolyte with different concentrations

is therefore easily decomposed at the surface, resulting in a decrease in the open circuit potential (OCP) of the cell [25]. In order to verify this, the cells with $LiBF_4$ electrolyte of different concentrations were charged to 5 V vs. Li/Li^+ and left for 24 h at room temperature. Figure 3a shows the voltage profile with storage time. It can be found that the OCP of the cell in the 1.4 M $LiBF_4$ is much higher than that in other concentration electrolytes. It may be that, in 1.4 M $LiBF_4$ electrolyte, a passivated film with protective function is formed on the surface of charged LNMO electrode. The formed protective film suppresses electrolyte decomposition, which is one of the main parasitic reactions taking place.

The potentiostatic hold means that, upon electrolyte oxidation and charge transfer of an electron from the electrolyte to the cathode, the transferred electron will be conducted through the external circuit and lead to a reduction reaction at the anode. In this way, the state of charge of the cathode, and thus the potential set by the potentiostat, can be maintained during electrolyte oxidation reactions [26]. Figure 3b presents the leakage current of LNMO/Li cells in the investigated electrolytes. The LNMO/Li cells were charged to 5 V and stay for 3 h after 3 charge/discharge cycles. From this perspective, the current in Fig. 3b could represent the electrolyte oxidation current. Clearly, the residual current of LNMO in 1.4 M $LiBF_4$ electrolytes is obviously lower than that of other concentration electrolytes, revealing that the decomposition of electrolyte could effectively suppress the oxidation of electrolyte [26]. Therefore, the cells with 1.4 M $LiBF_4$ electrolyte may show better electrochemical performance.

Cycling and rate performances of the cell with different electrolytes

Figure 4a shows the cycling performance and the coulombic efficiency of the LNMO/Li half cells in the different concentrations of $LiBF_4$ electrolyte at room temperature. After

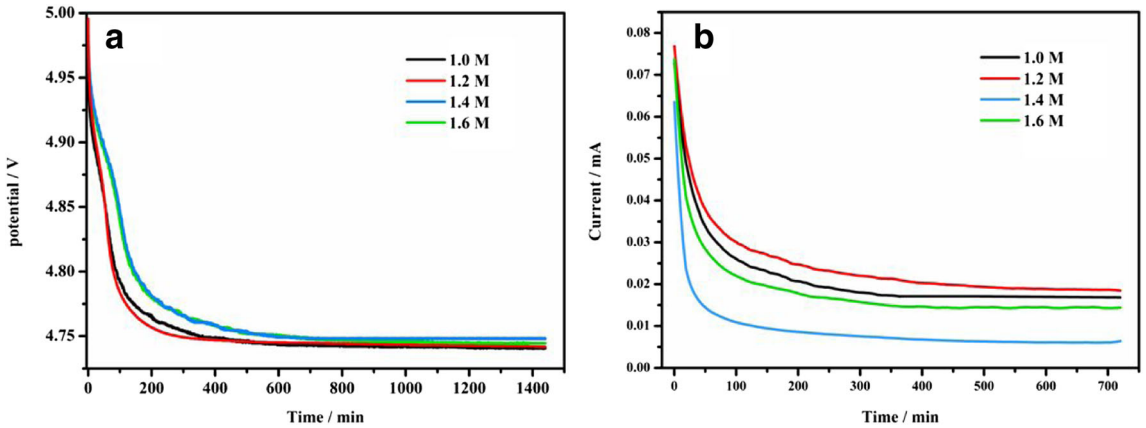

Fig. 3 The OCP (**a**) and leakage current (**b**) vs. time of LNMO/Li cells in different electrolytes

activation of several cycles at low current density, the half cells were charged at 1 C rate between 3.0 V and 5.0 V. We can clearly distinguish that the cyclic performance of the cell with 1.4 M $LiBF_4$ electrolyte is superior to that of other electrolytes in Fig. 4a. The cell with 1.4 M $LiBF_4$ electrolyte delivers 118.1 mAh g^{-1} after 100 cycles and maintains 92.2% of its initial capacity at 1 C, while the capacity retentions are 90.4, 81.7, and 91.1% for the 1, 1.2, and 1.6 M $LiBF_4$ electrolytes, respectively.

It can be found that the first cycle coulombic efficiencies of all cells with different electrolytes are less than 80%, suggesting that there is significant oxidation of the $LiBF_4$ and solvents on the first cycle. After activation cycles, the coulombic efficiencies are improved for all electrolytes (> 95%), indicating that the cathode surface has been passivated. One difference is that the coulombic efficiency significantly declined for the cells with 1.0, 1.2, and 1.6 M $LiBF_4$ electrolyte at 67th, 50th, and 40th cycle, respectively, whereas that of the cell with 1.4 M $LiBF_4$ electrolyte steadily increases and maintains at 96% after 100 cycles. It demonstrates that the cell with 1.4 M $LiBF_4$ electrolyte has much more stable cycling performance than that of other concentration electrolytes.

The rate capability of LNMO/Li half cells with different concentrations of $LiBF_4$ electrolyte in the voltage of 3.5 V–5.0 V from 0.2 C to 5.0 C is shown in Fig. 4b. The specific discharge capacities gradually decreased with the increase of the applied current densities for all the cells. Obviously, LNMO/Li cell with 1.4 M $LiBF_4$ electrolyte has an excellent rate capability, delivering a high specific discharge capacity of 111.2 mAh g^{-1} at 5 C, which is 83% of the discharge capacity at 0.5-C rate. The possible reason might be the relatively low film resistance of LNMO/Li cell with 1.4 M $LiBF_4$ electrolyte. Therefore, using 1.4 M $LiBF_4$ electrolyte can significantly improve the electrochemical performance of LNMO materials under high voltage.

The charge-discharge curve and EIS testing

Electrochemical tests were performed at room temperature to investigate the effect of $LiBF_4$ salt concentration in electrolyte on the electrochemical performance of LNMO cathode. Figure 5 shows the charge-discharge curves of LNMO cathodes between 3.5 and 5 V vs. Li/Li^+. In Fig. 5a, the specific capacities of samples prepared with 1.0, 1.2, 1.4, and 1.6 M

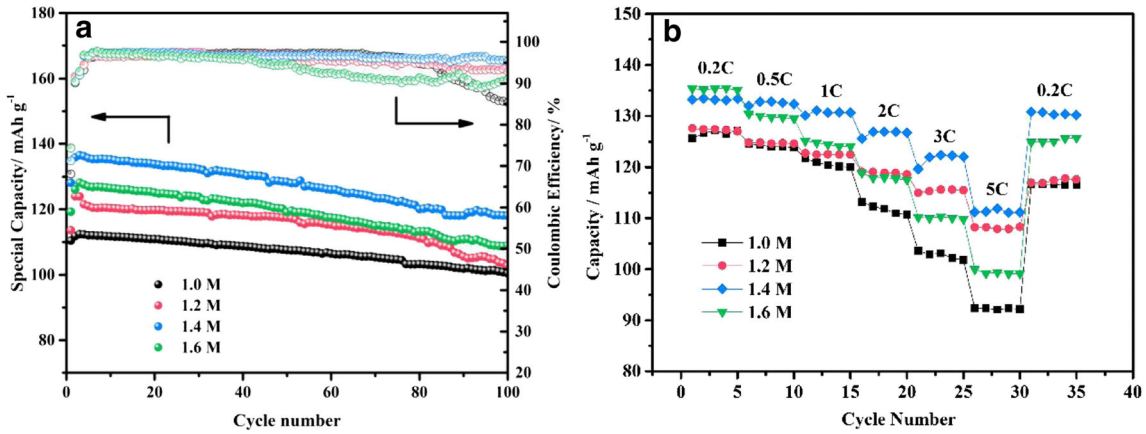

Fig. 4 Cycling (**a**) and rate (**b**) performance of the cell with different electrolytes

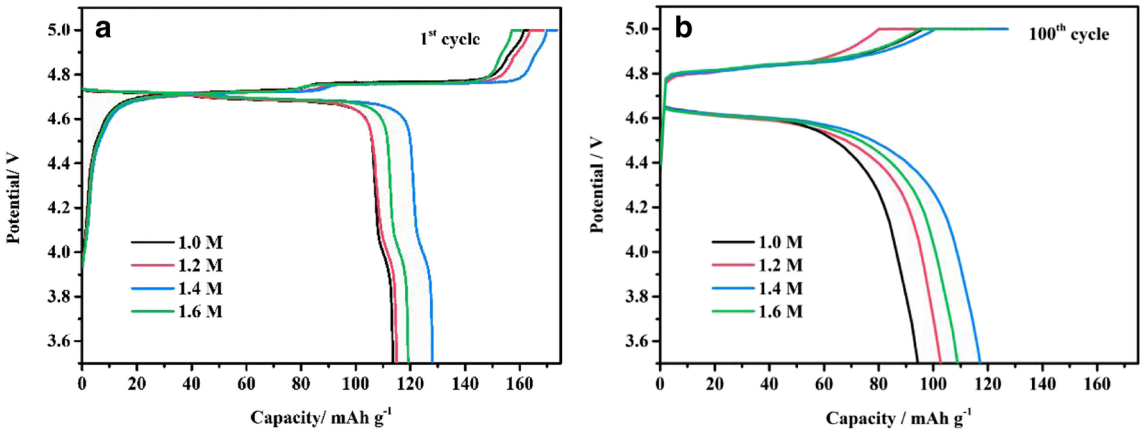

Fig. 5 The 1st (**a**) and 100th (**b**) charge-discharge curve of the cell with the different electrolytes

$LiBF_4$ salt concentrations in the first cycle are 113.6, 115, 128.1, and 119.2 mAh g^{-1}, respectively. In the initial anodic scan, there is a minor oxidation peak at 4.05 V and a major oxidation doublet at 4.74 V and 4.81 V, corresponding to the oxidation of Mn^{3+} to Mn^{4+}, Ni^{2+} to Ni^{3+}, and Ni^{3+} to Ni^{4+}, respectively. The cathodic peaks at 4.63 and 3.97 V are caused by the reduction of Ni^{4+} and Mn^{4+}, respectively [14].

From Fig. 5b, it can be seen that the specific capacities of samples prepared with 1.0, 1.2, 1.4, and 1.6 M $LiBF_4$ salt concentrations at the 100th cycle are 94.1, 102.7, 118.1, and 108.9 mAh g^{-1}. Throughout the long-term cycling, it seemed that the capacities of all the samples faded with the cycle number. However, it was noteworthy that the cell with 1.4 M $LiBF_4$ electrolyte degraded with the lowest rate and retained more than 92.2% of its initial capacity, as shown in Fig. 4a. The loss of discharge capacity from the 1st cycle to the 100th cycle is greater in the 1.4 M $LiBF_4$ electrolyte than in other electrolytes. On the other hand, by differentiating the charge-discharge profiles, the positive shift of voltage was clarified. The peak position corresponding to the plateaus (Ni^{2+}/Ni^{3+} or Ni^{3+}/Ni^{4+}) shifts with the cycle number, which means electrode kinetic is more sluggish with cycle number. Additionally, the SEI formed by the oxidation of $LiBF_4$ in 1.4 M $LiBF_4$ electrolyte may be more stable at high voltage and more effective in conducting lithium ions.

The impedance spectra of LMNO/Li with the different electrolytes after 1st (Fig. 6a) and 100th (Fig. 6b) cycles and the fitted equivalent circuit are shown in Fig. 6. Rs represents the ohmic resistance (a high-frequency tail at frequencies > 25 kHz). R_f and CPE_f are the resistance and constant phase elements of the solid-state interface film formed on the electrode surface (a high-frequency arc with a maximum located in the range of 10 to 1 kHz); Rct and CPE_{ct} are the charge transfer resistance and constant phase elements (a mid-frequency arc with a maximum located in the range of 100 to1 Hz). Ws is the Warburg resistance (a tail at frequencies < 1 Hz). The work potential of the cells was measured by half an hour, and then, the cells were tested impedance after the potential stability [27].

It confirms that the $LiBF_4$ participates in the formation of passivation film in Fig. 6a. The R_f value of the cell with 1.4 M $LiBF_4$ electrolyte is lower than that of other electrolytes after the first cycle, as shown in Table 1. This can be explained that the surface film resistance can be controlled by the reactivity of the electrolyte in the LSV data [28]. The lower R_f value implied that the film would be either thinner or less resistive [1]. After 100 cycles, although the surface film resistances of four cells are increased compared with those after the first cycle in Fig. 6b, the cells with 1.4 M $LiBF_4$ electrolyte showed a low surface film resistance than those of other electrolytes as shown in Table 2. Those impedance differences suggest that the surface film formed on the surface of the electrode with 1.4 M $LiBF_4$ is more stable, avoiding the continued growth of the surface layer [21]. The result also matches with the cycling and rate performance results shown in Fig. 4. The improved Li-ion conduction led to higher coulombic efficiency in the extended cycle, where the Li-ion batteries easily become detrimental.

Surface morphology and structure of cycled LNMO electrode

SEM analysis was applied to investigate the morphology of pristine cathode material and LNMO cathode materials removed from the cells after 100 charge-discharge cycles. Figure 7 presents the SEM images of the fresh and cycled LNMO electrodes. In Fig. 7a, the pristine cathode material is very fine and octahedral LNMO nanoparticles are obtained. The pristine cathode material shows a smooth surface on the individual LNMO grains with octahedral and truncated structure [29]. Comparing to the fresh electrode, the LNMO particle surface is apparently covered with amorphous small spherulites which may be the oxidation products of electrolyte during charge-discharge cycles for all the cathode materials. For the cell with 1.6 M $LiBF_4$ electrolyte (Fig. 7e), an increase in

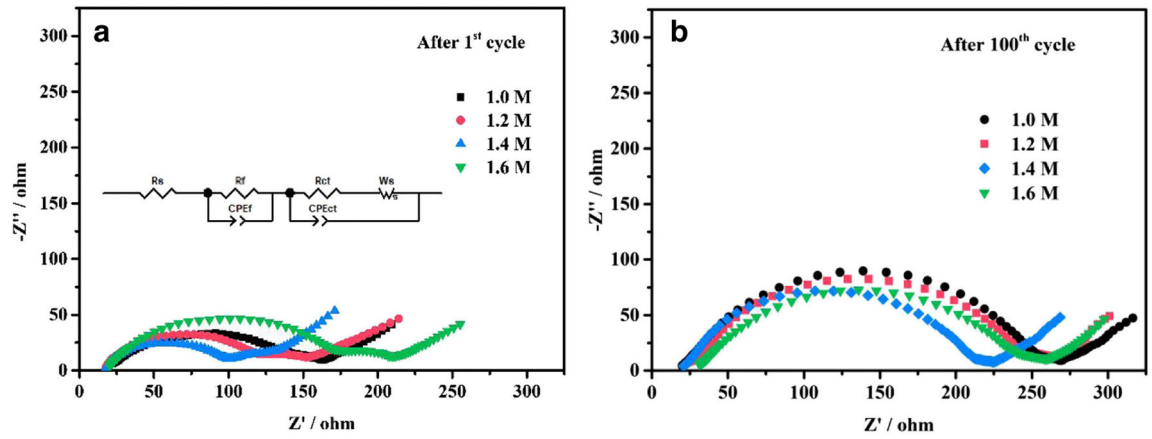

Fig. 6 The EIS of the cell with different electrolytes after 1st (**a**) and 100th (**b**) cycle

salt concentration of electrolyte has an excessively unfavorable effect on cathode material because of formation of SEI layer with low conductivity, which causes an increase in Rct value of this sample according to impedance spectra of Fig. 6. For the cell with 1.4 M $LiBF_4$ electrolyte (Fig. 7d), it can be seen that a compact and smooth protective film covers the surface of cathode, which implies that $LiBF_4$ either can passivate the surface of LNMO by forming a robust surface film or can not only keep cell impedance low and reduce dissolution of transition metal but also provide more smooth Li^+ ion diffusion.

In order to investigate the effect of the concentration of $LiBF_4$ in electrolyte solutions on the cathode performances, Raman spectra of the LNMO electrode after 100 cycles are conducted and shown in Fig. 8a. According to the factor group analysis [30], the irreversible representation of ordered spinel "$LiNi_{0.5}Mn_{1.5}O_4$" ($P4_332$) is given by $\Gamma P4_332 = 6A_1(\text{Raman}) + 14E_g(\text{Raman}) + 20F_1(\text{IR}) + 22F_2(\text{Raman})$. For the pristine LNMO, strong bands at around 470 cm^{-1} can be originated from the A_1 (Mn–O stretching) modes, and the bands at 496 and 399 cm^{-1} can be assigned to the F_2 and E_g modes (the Ni^{2+}–O stretching), respectively [31]. Simultaneously, the peak positions of the cathodes taken out from the cells prepared with 1.0, 1.2, and 1.6 M electrolytes show red shift to some extent compared with the pristine cathode material. Such phenomenon displays the weaker interaction between Mn and O ions, which may have some damage to the electrochemical performance [32]. Raman results are compatible with the electrochemical test results that the cells appear certain capacity fades. By comparison, the peak positions of the cathodes from the cells with 1.4 M $LiBF_4$ electrolyte displayed a smaller blue shift. Such a phenomenon displays the stronger interaction between Mn and O ions, which may lead to better electrochemical performance than that of the other cathode materials with worse discharge capacity [32]. Additionally, the peak intensity of the cell with 1.4 M $LiBF_4$ electrolytes is lower than those of the electrodes with other $LiBF_4$ concentrations. This Raman signal intensity difference suggests that it has a strong correlation with sample SEI thickness [33]. In the 1.0, 1.2, and 1.6 M $LiBF_4$ electrolyte, the SEI film thickness is higher than that in the 1.4 M $LiBF_4$ electrolyte. The observed Raman results indicate that a more thin and stable SEI film is formed on the LNMO electrode in 1.4 M $LiBF_4$ electrolyte.

The FTIR spectra of the pristine and cycled LNMO electrodes are presented in Fig. 8. For the pristine material (Fig. 8a), the spectrum is nearly featureless in most of the relevant range, except at around 650–450 cm^{-1} corresponding to the M-O vibrations in the spinel oxide [31]. Differently, the spectra of the cycled samples have abundant absorption peaks at 1515, 1436, and 863 cm^{-1}, corresponding to the electrolyte decomposition products, which generally consist of lithium alkyl carbonate (ROCOOLi), lithium carbonate (Li_2CO_3), lithium fluoride (LiF), and so on [34, 35]. The spectral features of the charged samples are also slightly different from that of the pristine electrode, indicating that the cathode particles are

Table 1 Fitted resistance values of the spectra shown in Fig. 6a

$LiBF_4$ concentration	R_s (Ω)	R_f (Ω)	R_{ct} (Ω)
1.0 M	12.24	132.7	70.56
1.2 M	16.08	97.72	53.48
1.4 M	15.98	84.04	29.09
1.6 M	17.79	160.6	32.93

Table 2 Fitted resistance values of the spectra shown in Fig. 6b

$LiBF_4$ concentrations	R_s (Ω)	R_f (Ω)	R_{ct} (Ω)
1.0 M	21.69	125.6	148.1
1.2 M	20.9	111	129.4
1.4 M	17.37	92.51	57.13
1.6 M	28.35	115.9	120.2

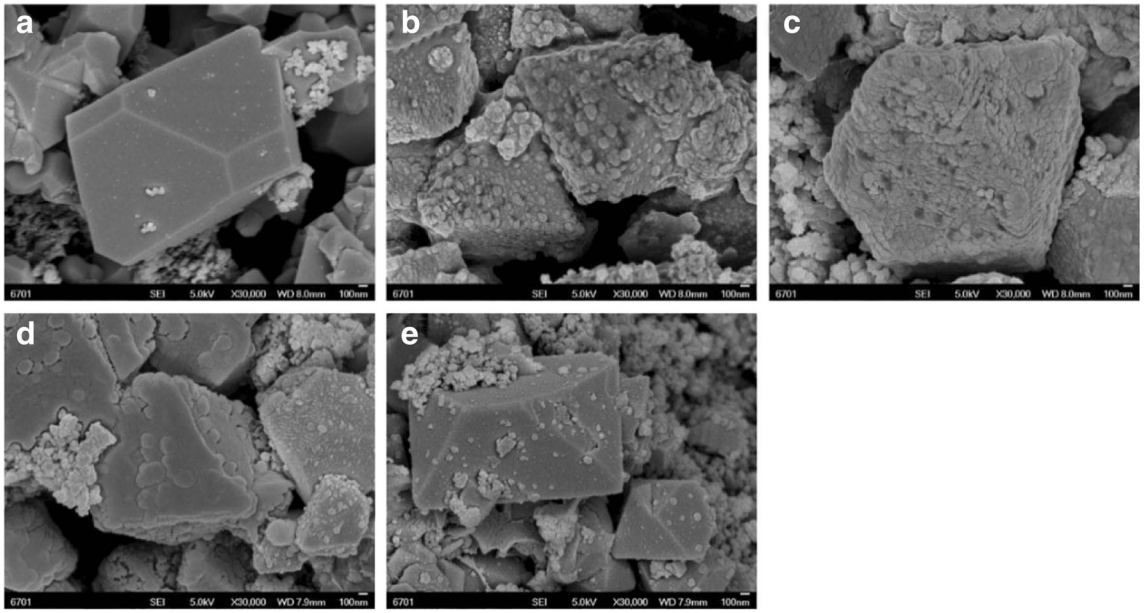

Fig. 7 The SEM images of pristine (**a**) and cycled electrode in 1.0 (**b**), 1.2 (**c**), 1.4 (**d**), and 1.6 M (**e**) $LiBF_4$ electrolytes

surrounded by some organic/inorganic compounds caused by the electrolyte decomposition reaction as well as the presence of the electrolyte components [36]. The FTIR spectrum of the cycled cathode with electrolyte containing 1.4 M $LiBF_4$ electrolyte has a new peak at 1041 cm^{-1} which is assigned to the υ(B-F) from the BF_4^- [37]. A small peak at 1600 cm^{-1} corresponds to υ (CO_2), a coordination type C–O bond, suggesting a metal organic salt such as RCO_2M (M=Ni, Mn and/or Li) [37].

According to the above discussions, the cell with 1.4 M $LiBF_4$-EC/DEC (1:5) electrolyte shows excellent electrochemical performance which may be ascribed to its peculiar solution structure: (i) all solvents and BF_4^- anions are strongly coordinated with Li^+ cations; thus, the probability of coordination with other metal cations is much lower; (ii) the resulting reinforced three-dimensional network structure further retards the diffusion rate of the metal cations, particularly, those with multiple charge [38].

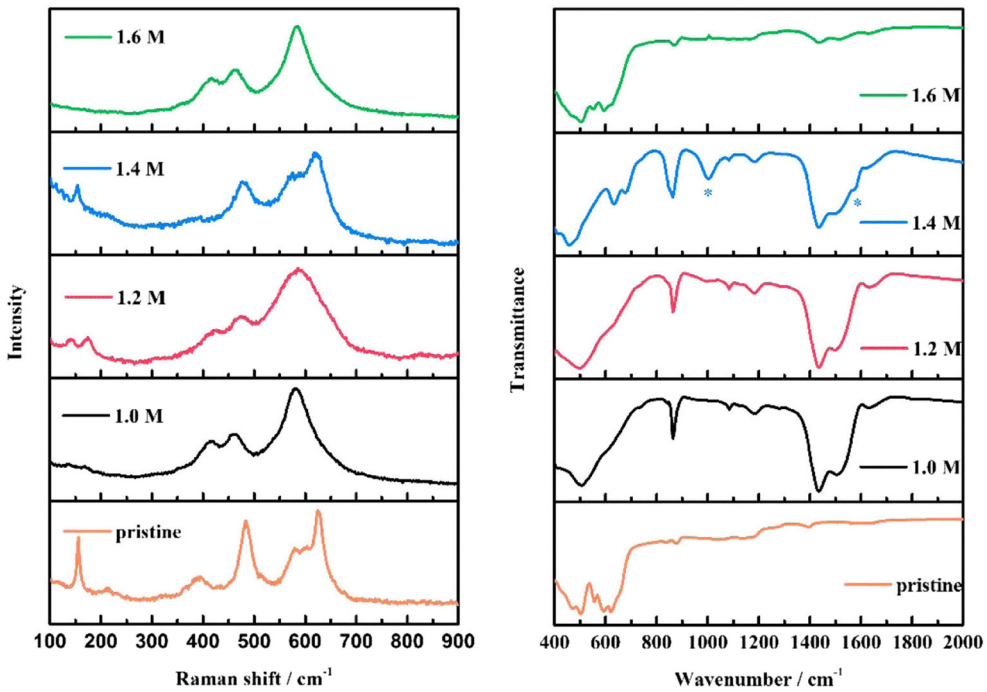

Fig. 8 The Raman (**a**) and FTIR (**b**) spectra of pristine and cycled electrode in different electrolytes

Conclusions

The finding of appropriate electrolytes and applying them to lithium-ion batteries are of special interest. $LiBF_4$ has often been studied as a replacement for $LiPF_6$ due to its particular advantages. In this work, various concentrations of $LiBF_4$-based electrolyte solutions were prepared for high-voltage LIBs. Electrochemical test results show that elaborately prepared 1.4 M $LiBF_4$-EC/DEC (1:5) electrolyte provides high electrochemical capacity and favorable rate performance for the high-voltage $LiNi_{0.5}Mn_{1.5}O_4$ cathode material. We believe that the formation of thin and stable SEI film on the surface of LNMO electrode plays an important role in suppressing continuous decomposition of electrolyte.

Funding information This work was supported by the Natural Science Foundation of China (no. 21766017 and 21566021), the Chinese Academy of Sciences "Light in the West" - Western Young Scholars Project, and the Science and Technology Planning Project of Gansu Province (No. 18JR3RA160).

References

1. Kim S, Kim M, Choi I, Kim JJ (2016) Quercetin as electrolyte additive for $LiNi_{0.5}Mn_{1.5}O_4$ cathode for lithium-ion secondary battery at elevated temperature. J Power Sources 336:316–324
2. Son IH, Park K, Park JH (2017) Improvement in high-voltage and high rate cycling performance of nickel-rich layered cathode materials via facile chemical vapor deposition with methane. Electrochim Acta 230:308–315
3. Yamagiwa K, Morita D, Yabuuchi N, Tanaka T, Fukunishi M, Taki T, Watanabe H, Otsuka T, Yano T, Son JY (2015) Improved high-temperature performance and surface chemistry of graphite/$LiMn_2O_4$ Li-ion cells by fluorosilane-based electrolyte additive. Electrochim Acta 160:347–356
4. Xiang K, Wang X, Chen M, Shen Y, Shu H, Yang X (2017) Industrial waste silica preparation of silicon carbide composites and their applications in lithium-ion battery anode. J Alloys Compd 695:100–105
5. Maeyoshi Y, Miyamoto S, Noda Y, Munakata H, Kanamura K (2017) Effect of organic additives on characteristics of carbon-coated $LiCoPO_4$ synthesized by hydrothermal method. J Power Sources 337:92–99
6. Truong Q, Devaraju M, Honma I (2014) Benzylamine-directed growth of olivine-type $LiMPO_4$ nanoplates by a supercritical ethanol process for lithium-ion batteries. J Mater Chem A 2:17400–17407
7. Devaraju MK, Truong QD, Hyodo H, Sasaki Y, Honma I (2015) Synthesis, characterization and observation of antisite defects in $LiNiPO_4$ nanomaterials. Sci Rep 5:11041
8. Mun J, Park JH, Choi W, Benayad A, Park JH, Lee JM, Doo SG, Oh S (2014) New dry carbon nanotube coating of over-lithiated layered oxide cathode for lithium ion batteries. J Mater Chem A 2:19670–19677
9. Rui X, Yan Q, Skyllas-Kazacos M, Lim TM (2014) $Li_3V_2(PO_4)_3$ cathode materials for lithium-ion batteries: a review. J Power Sources 258:19–38
10. Feng J, Huang Z, Guo C, Chernova NA, Upreti S, Whittingham MS (2013) An organic coprecipitation route to synthesize high voltage $LiNi_{0.5}Mn_{1.5}O_4$. ACS Appl Mater Interfaces 5:10227–10232
11. Mao J, Dai K, Xuan M, Shao G, Qiao R, Yang W, Battaglia VS, Liu G (2016) Effect of chromium and niobium doping on the morphology and electrochemical performance of high-voltage spinel $LiNi_{0.5}Mn_{1.5}O_4$ cathode material. Solid State Ionics 292:70–74
12. Kraytsberg A, Ein-Eli Y (2012) Higher, stronger, better…a review of 5 volt cathode materials for advanced lithium-ion batteries. Adv Energy Mater 2:922–939
13. Liu D, Zhu W, Trottier J, Gagnon C, Barray F, Guerfi A, Mauger A, Groult H, Julien CM, Goodenough JB (2013) Spinel materials for high-voltage cathodes in Li-ion batteries. RSC Adv 4:154–167
14. Li Y, Wan S, Veith GM, Unocic RR, Paranthaman MP, Dai S, Sun XG (2016) A novel electrolyte salt additive for lithium-ion batteries with voltages greater than 4.7 V. Adv Energy Mater 7:1061397
15. Zhang L, Chai L, Li Z, Shen M, Zhang X, Battaglia VS, Stephenson T, Zheng H (2014) Synergistic effect between lithium bis(fluorosulfonyl)imide (LiFSI) and lithium bis-oxalato borate (LiBOB) salts in $LiPF_6$-based electrolyte for high-performance Li-ion batteries. Electrochim Acta 127:39–44
16. Karaal Ş, Köse H, Aydin AO, Akbulut H (2015) The effect of $LiBF_4$ concentration on the discharge and stability of $LiMn_2O_4$ half cell Li ion batteries. Mater Sci Semicond Process 38:397–403
17. Zhang S, Xu K, Jow T (2003) Low-temperature performance of Li-ion cells with a $LiBF_4$ -based electrolyte. J Solid State Electrochem 7:147–151
18. Jow TR, Ding MS, Xu K, Zhang SS, Allen JL, Amine K, Henriksen GL (2003) Nonaqueous electrolytes for wide-temperature-range operation of Li-ion cells. J Power Sources 343-348:s119–s121
19. Ellis LD, Xia J, Louli AJ, Dahn JR (2016) Effect of substituting $LiBF_4$ for $LiPF_6$ in high voltage lithium-ion cells containing electrolyte additives. J Electrochem Soc 163:A1686–A1692
20. Doi T, Shimizu Y, Hashinokuchi M, Inaba M (2017) Low-viscosity γ-butyrolactone-based concentrated electrolyte solutions for $LiNi_{0.5}Mn_{1.5}O_4$ positive electrodes in lithium-ion batteries. Chemelectrochem 4:2398–2403
21. Doi T, Shimizu Y, Hashinokuchi M, Inaba M (2016) $LiBF_4$-based concentrated electrolyte solutions for suppression of electrolyte decomposition and rapid lithium-ion transfer at $LiNi_{0.5}Mn_{1.5}O_4$/electrolyte interface. J Electrochem Soc 163:A2211–A2215
22. Zheng J, Lochala JA, Kwok A, Deng ZD, Xiao J (2017) Research progress towards understanding the unique interfaces between concentrated electrolytes and electrodes for energy storage applications. Adv Sci 4:1700032
23. Doi T, Shimizu Y, Hashinokuchi M, Inaba M (2017) Dilution of highly concentrated $LiBF_4$/propylene carbonate electrolyte solution with fluoroalkyl ethers for 5-V $LiNi_{0.5}Mn_{1.5}O_4$ positive electrodes. J Electrochem Soc 164:A6412–A6416
24. Xu K (2014) Electrolytes and interphases in Li-ion batteries and beyond. Chem Rev 114:11503
25. Nie M, Xia J, Dahn JR (2015) Development of pyridine-boron trifluoride electrolyte additives for lithium-ion batteries. J Electrochem Soc 162:1186–1195
26. Tornheim A, He M, Su CC, Zhang Z (2017) The role of additives in improving performance in high voltage lithium-ion batteries with potentiostatic holds. J Electrochem Soc 164:A6366–A6372
27. Zhao Q, Zhang Y, Tang F, Zhao J, Li S (2017) Mixed salts of lithium difluoro (oxalate) borate and lithium tetrafluorobotate electrolyte on low-temperature performance for lithium-ion batteries. J Electrochem Soc 164:A1873–A1880
28. Dong Y, Young BT, Zhang Y, Yoon T, Heskett DR, Hu Y, Lucht BL (2017) Effect of lithium borate additives on cathode film formation in $LiNi_{0.5}Mn_{1.5}O_4$/Li cells. ACS Appl Mater Interfaces 9:20467
29. Yi TF, Mei J, Zhu YR (2016) Key strategies for enhancing the cycling stability and rate capacity of $LiNi_{0.5}Mn_{1.5}O_4$ as high-voltage cathode materials for high power lithium-ion batteries. J Power Sources 316:85–105

30. Wang L, Li H, Huang X, Baudrin E (2011) A comparative study of Fd-3m and P4332 "$LiNi_{0.5}Mn_{1.5}O_4$". Solid State Ionics 193:32–38
31. Amdouni N, Zaghib K, Gendron F, Mauger A, Julien CM (2006) Structure and insertion properties of disordered and ordered $LiNi_{0.5}Mn_{1.5}O_4$ spinels prepared by wet chemistry. Ionics 12:117–126
32. Dombaycıoğlu Ş, Köse H, Aydın AO, Akbulut H (2016) The effect of $LiBF_4$ salt concentration in EC-DMC based electrolyte on the stability of nanostructured $LiMn_2O_4$ cathode. Int J Hydrog Energy 41:9893–9900
33. Park Y, Su HS, Lee SM, Kim SP, Choi HC, Jung YM (2014) 2D Raman correlation analysis of formation mechanism of passivating film on overcharged $LiCoO_2$ electrode with additive system. J Mol Struct 1069:183–187
34. Ostrovskii D, Ronci F, Scrosati B, Jacobsson P (2001) A FTIR and Raman study of spontaneous reactions occurring at the $LiNi_yCo_{(1-y)}O_2$ electrode/non-aqueous electrolyte interface. J Power Sources 94:183–188
35. Matsui M, Dokko K, Kanamura K (2008) Dynamic behavior of surface film on $LiCoO_2$ thin film electrode. J Power Sources 177:184–193
36. Park Y, Kim NH, Cho SB, Kim JM, Kim GC, Min SK, Lee SM, Eom IY, Choi HC, Jung YM (2010) Characterization of the passivating layer on $Li[Ni_{0.31}Co_{0.32}Mn_{0.28}Al_{0.09}]O_2$ cathode in the overcharge state. J Mol Struct 974:139–143
37. Song SW, Richardson TJ, Zhuang GV, Devine TM, Evans JW (2004) Effect on aluminum corrosion of $LiBF_4$ addition into lithium imide electrolyte; a study using the EQCM. Electrochim Acta 49:1483–1490
38. Wang J, Yamada Y, Sodeyama K, Chiang CH, Tateyama Y, Yamada A (2016) Superconcentrated electrolytes for a high-voltage lithium-ion battery. Nat Commun 7:12032